Phase and group velocities for correlation spreading in the Mott phase of the Bose-Hubbard model in dimensions greater than one

Ali Mokhtari-Jazi, Matthew R. C. Fitzpatrick, and Malcolm P. Kennett
Department of Physics, Simon Fraser University, 8888 University Drive, Burnaby, British Columbia, Canada V5A 1S6

(Received 5 August 2020; accepted 10 February 2021; published 26 February 2021)

Lieb-Robinson and related bounds set an upper limit on the speed at which information propagates in nonrelativistic quantum systems. Experimentally, light-cone-like spreading has been observed for correlations in the Bose-Hubbard model (BHM) after a quantum quench. Using a two-particle irreducible (2PI) strong-coupling approach to out-of-equilibrium dynamics in the BHM we calculate both the group and phase velocities for the spreading of single-particle correlations in one, two, and three dimensions as a function of interaction strength. Our results are in quantitative agreement with measurements of the speed of spreading of single-particle correlations in both the one- and two-dimensional BHM realized with ultracold atoms. They also are consistent with the claim that the phase velocity rather than the group velocity was observed in recent experiments in two dimensions. We demonstrate that there can be large differences between the phase and group velocities for the spreading of correlations and explore how the anisotropy in the velocity varies across the phase diagram of the BHM. Our results establish the 2PI strong-coupling approach as a powerful tool to study out-of-equilibrium dynamics in the BHM in dimensions greater than one.

DOI: 10.1103/PhysRevA.103.023334

I. INTRODUCTION

Ultracold atoms in optical lattices provide a versatile setting to investigate out-of-equilibrium dynamics in interacting quantum systems [1–8]. Atomic realizations of the Bose Hubbard model (BHM) [9], a minimal model describing interacting bosons in an optical lattice [10], have also been proposed as quantum simulators in dimensions higher than one [11,12]. Understanding how information propagates in these systems provides insights that can help the engineering of efficient quantum channels necessary for fast quantum computations [13]. In this work we focus on the question of how the speed of information propagation depends on dimensionality and model parameters in the BHM and whether theory can match experimental observations, particularly for two dimensions.

The existence of a bound on the group velocity of the spreading of correlations in nonrelativistic quantum spin systems with finite-range interactions was demonstrated by Lieb and Robinson [14]. For bosonic systems with infinite-dimensional Hilbert space and unbounded Hamiltonians, analogous bounds can be found in some cases [15], but it is also possible to construct models with accelerating excitations [16]. Additionally, Lieb-Robinson bounds have been derived for spin-boson models relevant for trapped ions [17]. In the specific case of the BHM, a bound has been derived for a specific class of initial states [18], but there are no rigorous results for the spreading of correlations in, e.g., a Mott state. Experimentally, *in situ* imaging techniques such as quantum gas microscopes [19,20] have enabled the demonstration of light-cone-like spreading [21] of correlations for bosons in a one-dimensional optical lattice simulating the BHM.

There are multiple theoretical methods that enable the calculation of dynamical correlations in the BHM in one dimension, including exact diagonalization (ED) and time-dependent density-matrix renormalization-group methods (t-DMRG) [21–30]. However, these tools are not effective for calculating the spreading of correlations in higher dimensions. Theorists have responded to this challenge by using a variety of methods to study the spreading of correlations in the BHM in two dimensions, including considering Gutzwiller mean-field theory with perturbative corrections [31–34], time-dependent variational Monte Carlo [35] and doublon-holon pair theories [36]. We employ a two-particle irreducible (2PI) [37,38] strong-coupling approach to the BHM developed by two of us that uses a closed time path method to treat out-of-equilibrium dynamics (details can be found in Refs. [39–42] and Appendix A) allowing accurate calculation of the speed at which correlations spread in dimensions higher than one. This approach is exact in both the weak- and strong-interaction limits and is applicable for small average particle number per site, $\bar{n}$. In Ref. [40] two of us used this approach to obtain 2PI equations of motion for single-particle correlations. These equations of motion are not amenable to numerical solution due to the presence of multiple time integrals, but taking a low-energy limit yields an effective theory (ET) that gives predictions that match exact results in one dimension [41].

Our work is motivated by recent experiments reported by Takasu *et al.* [12], who studied the spreading of single-particle correlations for bosonic atoms confined in an optical lattice in one, two, and three dimensions after a quench in the optical lattice depth starting from a Mott-insulating state. In terms of the BHM, these quenches correspond to different values of the ratio U/J_f, where U is the characteristic interaction energy scale and J_f is the final value of the characteristic

 ©2021 American Physical Society

hopping energy scale J. In one dimension they considered parameters well in the Mott phase [$U/J_f = 6.8$, compared with the critical value $(U/J)_c^{1d} = 3.4$], and in two dimensions they considered parameters close to the transition to a superfluid [$U/J_f = 19.6$ compared with the critical value of $(U/J)_c^{2d} = 16$]. Defining the correlation wavefront as the first peak in the time evolution of the single-particle correlation function at each particle separation distance, Takasu *et al.* found the wavefront to propagate in one dimension with a velocity of $v_{\text{peak}} = 5.5(7)Ja/\hbar$, where a is the lattice spacing, in accord with previous experimental [21] and theoretical results [21,27,30,41].

Takasu *et al.* [12] reported the first measurements of propagation speeds in two dimensions, $v_{\text{peak}} = 13.7(2.1)Ja/\hbar$ (obtained from the first peak in the single-particle correlations) and $v_{\text{trough}} = 10.2(1.4)Ja/\hbar$ (obtained from the first trough after the first peak). These values, especially v_{peak}, are considerably larger than the value of $v_{\text{max}}^{2d} = 8.4Ja/\hbar$ that Takasu *et al.* expected based on doublon-holon effective theories [21,27]. We note that Refs. [21,27] studied the one-dimensional Bose Hubbard model and made use of the Jordan-Wigner transformation—a one-dimensional technique. The only derivation for v_{max}, which Takasu *et al.* state can be interpreted as a Lieb-Robinson-like bound (i.e., corresponding to the group velocity) in dimensions larger than one, that we are aware of is that of Krutitsky *et al.* [33]. However, their result agrees with the v_{max}^{2d} expression given by Takasu *et al.* only to zeroth order in J/U. Moreover, the expression obtained by Krutitsky *et al.* is only valid deep in the Mott-insulating regime, so is not applicable to the U/J values considered by Takasu *et al.* that are of interest here. Takasu *et al.* argue that they measured the phase rather than the group velocity; these were identified as being distinct for the BHM in one dimension in Ref. [30].

In this paper we solve the equations of motion for our 2PI ET and calculate the group and phase velocities for the spreading of single-particle correlations in the BHM after a quench in one, two, or three dimensions.

Our main results are as follows: (i) We obtain the group and phase velocities for correlation spreading throughout the Mott phase of the BHM in one, two, and three dimensions. (ii) We obtain quantitative agreement between the phase and group velocities of single-particle correlations in the one- and two-dimensional BHM calculated using our ET and velocities measured experimentally in Refs. [12,21]. (iii) We confirm that the phase rather than the group velocity was measured in two dimensions in Ref. [12]. (iv) We track the evolution of anisotropy in the phase and group velocities in the BHM in both two and three dimensions.

This paper is structured as follows: In Sec. II we introduce the BHM and our methodology, in Sec. III we present our results for one, two, and three dimensions, and in Sec. IV we discuss our results and conclude.

II. MODEL AND METHODOLOGY

We study the BHM on a d-dimensional cubic lattice, with $d = 1$, 2, and 3, for which the Hamiltonian is

$$\hat{H}_{\text{BHM}} = -\sum_{\langle i,j\rangle} J(t)\left(\hat{a}_{\mathbf{r}_i}^\dagger \hat{a}_{\mathbf{r}_j} + \hat{a}_{\mathbf{r}_j}^\dagger \hat{a}_{\mathbf{r}_i}\right) - \mu \sum_i \hat{n}_{\mathbf{r}_i} + \frac{U}{2}\sum_i \hat{n}_{\mathbf{r}_i}\left(\hat{n}_{\mathbf{r}_i} - 1\right), \tag{1}$$

where $\hat{a}_{\mathbf{r}_i}^\dagger$ and $\hat{a}_{\mathbf{r}_i}$ are bosonic creation and annihilation operators, respectively, and $\hat{n}_{\mathbf{r}_i}$ is the number operator, on site i (located at $\mathbf{r}_i$), U is the interaction strength, and μ is the chemical potential. We restrict the hopping to be between nearest-neighbor sites and allow the magnitude $J(t)$ to be time dependent, as required for a quench protocol. Our ET and the equations of motion for the single-particle correlations were derived in Refs. [40,41]. We calculate the same quantity that was measured by Takasu *et al.*, the single-particle density matrix

$$\rho_1(\Delta\mathbf{r} = \mathbf{r}_i - \mathbf{r}_j, t) = \left\langle \hat{a}_{\mathbf{r}_i}^\dagger(t)\hat{a}_{\mathbf{r}_j}(t)\right\rangle, \tag{2}$$

which contains all the information about single-particle observables, and on a lattice can be written in the form

$$\rho_1(\Delta\mathbf{r}, t) = \frac{1}{N_s}\sum_{\mathbf{k}} \cos(\mathbf{k}\cdot\Delta\mathbf{r}) n_{\mathbf{k}}(t), \tag{3}$$

where N_s is the number of sites, and $n_{\mathbf{k}}(t)$ is the particle distribution over the quasimomentum $\mathbf{k}$ at time t, and $\Delta\mathbf{r}$ is the particle separation distance. $n_{\mathbf{k}}(t)$ is related to the density $n(t)$ via

$$n(t) = \frac{1}{N_s}\sum_{\mathbf{k}} n_{\mathbf{k}}(t). \tag{4}$$

Note that usually one would expect the total particle number to be conserved, but due to truncations in our ET, there are small fluctuations in the particle number that do not appear to affect the determination of the velocity at which correlations spread [41]. In addition to single-particle correlations, density-density correlations have also been considered in the literature [27,30]. Such correlations are not as easily accessible with our approach, but in the strong-coupling limit of the BHM, higher-order correlations contain the same information as single-particle correlations [27,41].

The protocol we follow is to start with $J/U = 0$ for a $\bar{n} = 1$ Mott phase and then ramp J to a final value J_f over a timescale τ_Q, with the timescale t_c marking the midpoint of the quench [41]. We solve the ET equations of motion to obtain $\rho_1(\Delta\mathbf{r}, t)$, from which we extract the group and phase velocities for the spreading of single-particle correlations. More details on the procedure we used can be found in Appendix B. We now discuss our results for one, two, and three dimensions in turn.

III. RESULTS

A. One dimension

We consider one-dimensional chains with 50 sites and periodic boundary conditions (PBCs). In previous work [41]

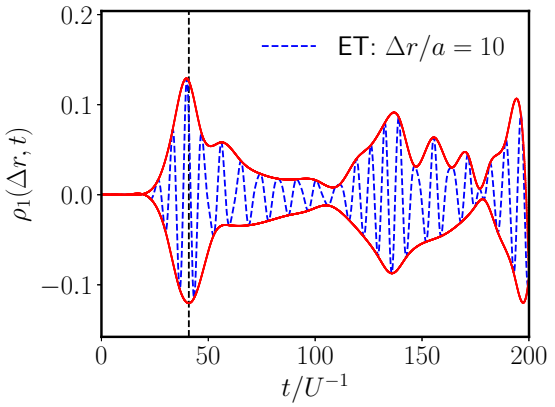

FIG. 1. Dynamics of $\rho_1(\Delta r, t)$ calculated from the ET in one dimension for $\Delta r/a = 10$. The envelope of the wave packet is shown in red and the center of the wave packet is marked by the dashed black vertical line. We use parameters $\beta U = 1000$, $U/J_f = 18.2$, $\mu/U = 0.4116$, $t_c/U^{-1} = 5$, $t_Q/U^{-1} = 0.1$, and $N_s = 50$.

we showed that the spreading of correlations calculated with our ET matches well with ED results in small systems and exact results for larger systems in one dimension. For a given U/J_f, we calculate $\rho_1(\Delta\mathbf{r}, t)$ and for each value of $\Delta\mathbf{r}$ we obtain the time-wise positions of the wave packet, and the largest peak [i.e., the point in time where $\rho_1(\Delta\mathbf{r}, t)$ takes its maximum value]. We track the propagation of the maximum peak of the $\rho_1(\Delta\mathbf{r}, t)$ time series to extract the phase velocity. To obtain the group velocity we first perform both linear and cubic interpolations to determine the upper and lower envelopes of $\rho_1(\Delta\mathbf{r}, t)$ and then average the centers of the pairs of upper and lower envelopes to identify the position of the wave packet. Full details of our procedure are given in Appendix B. An example of the envelope for $\rho_1(\Delta\mathbf{r}, t)$ is given in Fig. 1 for $\Delta r/a = 10$ and $U/J_f = 18.2$, with the time-wise position of the wave packet marked by a vertical dashed black line. By tracking the propagation of the wave packet, we can extract the group velocity for the spreading of single-particle correlations [41]. Figure 2 plots the times t/U^{-1} for the maximum peak and the wave packet to travel

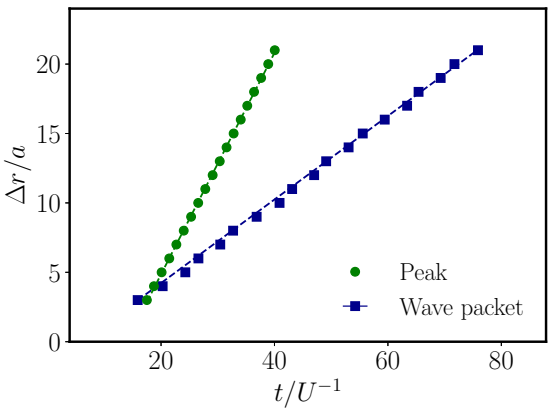

FIG. 2. Scatter plots of the time t/U^{-1} for the maximum peak (green) and the wave packet (blue) to travel a distance $\Delta\mathbf{r}/a$. Parameters are the same as in Fig. 1.

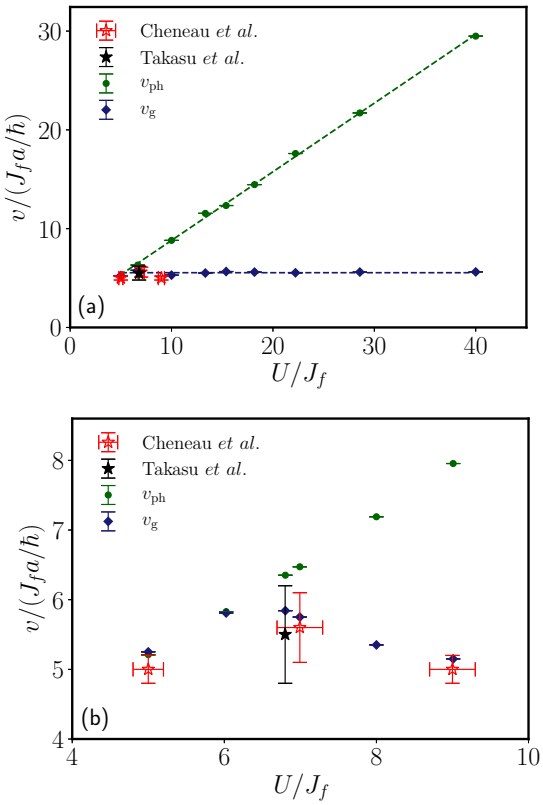

FIG. 3. (a) Phase velocity ($v_{\rm ph}$) and group velocity ($v_{\rm g}$) for single-particle correlations as a function of U/J_f for a 50-site chain. Experimental results from Cheneau *et al.* [21] and Takasu *et al.* [12] are also shown. The dashed lines are to guide the eye. (b) Comparison between experiment and theory in the range of U/J_f where experimental data are available.

a particle separation distance $\Delta r/a$ for the same parameters used in Fig. 1. By performing linear fits to the data in Fig. 2, we extract estimates for the phase and group velocities. The wave packets show less damping than those seen experimentally [12,21]. There are several possible sources for this discrepancy: on the theoretical side, there are higher-order terms in the 2PI expansion that lead to an imaginary part of the self-energy which should lead to damping [43]. We exclude these terms because they should be small in comparison with the terms that we keep, and in doing so the problem becomes more numerically tractable. Experimentally, sources of damping that are not included in our calculation, such as atom number fluctuations, may also be important.

We repeat the process illustrated in Figs. 1 and 2 throughout the Mott phase to determine the group and phase velocity at each value of U/J_f. These results and a comparison to the velocities determined experimentally in Refs. [12,21] are presented in Fig. 3. Note that the velocities obtained in Ref. [21] are actually for density-density correlations rather than single-particle correlations, but at strong coupling, these two correlations should spread with similar velocities [27,41]. Deep in the Mott-insulating phase, the phase velocity is much larger than the group velocity but the two velocities converge in the vicinity of the critical point. Our results are consistent with those recently obtained theoretically using matrix

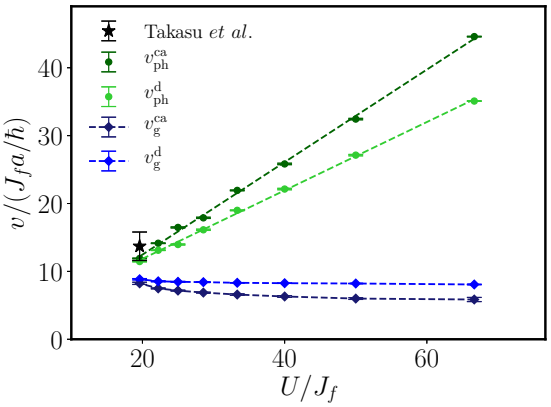

FIG. 4. Phase velocity $v_{\rm ph}$ and group velocity $v_{\rm g}$ along both the crystal axes (superscript ca) and along the diagonal (superscript d) as a function of U/J_f for the BHM in two dimensions. The peak velocity in the single-particle correlations determined by Takasu *et al.* [12] is also shown.

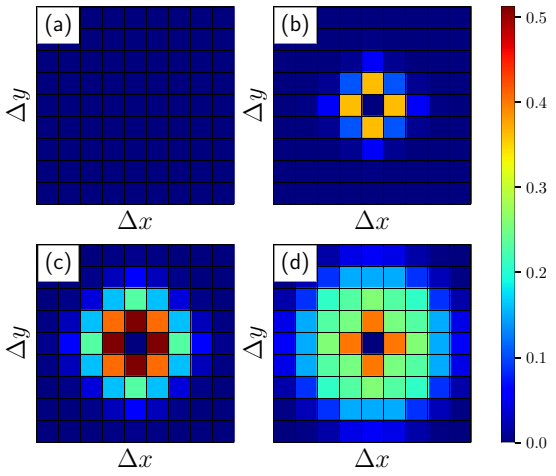

FIG. 5. Snapshots of $\rho_1(\Delta\mathbf{r}, t)$ at four times after the quench: (a) 0, (b) $0.12\hbar/J$, (c) $0.23\hbar/J$, and (d) $0.35\hbar/J$. The parameters used are $\beta U = 1000$, $U/J_f = 19.6$, $\mu/U = 0.4116$, and $N_s = 50$.

product states by Despres *et al.* [30]. Our results for the group velocity are consistent with measurements of the group velocity by Cheneau *et al.* [21] at several different values of U/J_f. Takasu *et al.* [12] identified their results with the group velocity, which agree with the value we compute for the group velocity. However, they used the position of the peak to determine the velocity, which would suggest they may have measured the phase velocity—they note that the two values are quite close for $U/J_f = 6.8$. The value we obtain for the phase velocity is just outside the error bars of Takasu *et al.*'s measurement, but given that we consider a uniform system, whereas the experiment is in a trap, it would appear that the results of Takasu *et al.* are not inconsistent with them having measured the phase velocity in one dimension. Having established that our ET reproduces existing experimental results for the group velocity and theoretical results obtained using essentially exact methods in one dimension, we now turn to two dimensions, where the phase velocity has not been previously considered theoretically.

B. Two dimensions

We consider a 50×50 lattice with PBCs and follow the same procedure as for one dimension to calculate $\rho_1(\Delta\mathbf{r}, t)$. As noted by previous authors, the spreading of correlations in two dimensions is anisotropic in both the Mott [33,41] and superfluid [35] regimes. We calculate the phase and group velocities as a function of U/J_f along both the crystal axes and the diagonals using the same protocol as for one dimension and present the results in Fig. 4. We consider parameters $\beta U = 1000$, $\mu/U = 0.4116$, $t_c/U^{-1} = 5$, and $t_Q/U^{-1} = 0.1$.

Takasu *et al.* [12] identified propagation velocities for single-particle correlations by fitting to the peak and the following trough in $\rho_1(\Delta\mathbf{r}, t)$ at each Δr. These values were $v_{\rm peak} = 13.7(2.1) J_f a/\hbar$ and $v_{\rm trough} = 10.2(1.4) J_f a/\hbar$ for $U/J_f = 19.6$. In Fig. 4 we show the group and phase velocities, evaluated along both the diagonals and the crystal axes in two dimensions. We used the peaks in $\rho_1(\Delta\mathbf{r}, t)$ to calculate the phase velocity and accordingly plot the value of Takasu *et al.* for $v_{\rm peak}$ in Fig. 4. For $U/J_f = 19.6$ we find the group velocity and phase velocity [determined using the peak in $\rho_1(\Delta\mathbf{r}, t)$] along the diagonals to be $v_{\rm g}^{\rm d} \simeq 8.8 J_f a/\hbar$ and $v_{\rm ph}^{\rm d} \simeq 11.5 J_f a/\hbar$ and along the crystal axes $v_{\rm g}^{\rm ca} \simeq 8.2 J_f a/\hbar$ and $v_{\rm ph}^{\rm ca} \simeq 11.9 J_f a/\hbar$ respectively. We also determined the phase velocity using the first trough after the peak in $\rho_1(\Delta\mathbf{r}, t)$ and obtained $v_{\rm ph}^{\rm ca} = 11.2 J_f a/\hbar$ and $v_{\rm ph}^{\rm d} = 11.0 J_f a/\hbar$, also consistent with experiment. This result indicates a strength of our method relative to the truncated Wigner approximation (TWA) used in Ref. [12], which failed to capture the locations of the correlation troughs. Our results are consistent with the statement of Takasu *et al.* that they measure the phase velocity rather than the group velocity for the spreading of correlations.

We find both the group and phase velocities to be anisotropic, but with opposite sense—the velocity along the diagonals is larger than along the crystal axis for the group velocity and the converse for the phase velocity. The degree of anisotropy of both the phase and group velocities in two dimensions is maximum at large values of U/J_f and the velocities are close to isotropic as U/J_f approaches the critical value of $(U/J)_c^{2d} = 16$. Theoretical calculations for the group velocity in the superfluid regime [35] indicate that the superfluid also displays anisotropic spreading of correlations, with the opposite sense to that in the Mott regime. In Fig. 5 we show the spreading of $\rho_1(\Delta\mathbf{r}, t)$ at four times after the quench, for Euclidean distances $\Delta \leqslant 4$, as measured by Takasu *et al.* (we display correlations for the same times as those shown in Ref. [12]). The magnitude of $\rho_1(\Delta\mathbf{r}, t)$ we find from our ET is about twice the amplitude at the peak observed in experiment or ED calculations in small systems, but the phase of $\rho_1(\Delta\mathbf{r}, t)$ appears to be considerably more accurate. At larger values of U/J_f the ET accurately reproduces ED results, as illustrated in Appendix B.

C. Three dimensions

We followed a procedure similar to that used for one and two dimensions to determine the group and phase velocities for the spreading of correlations in three dimensions for a

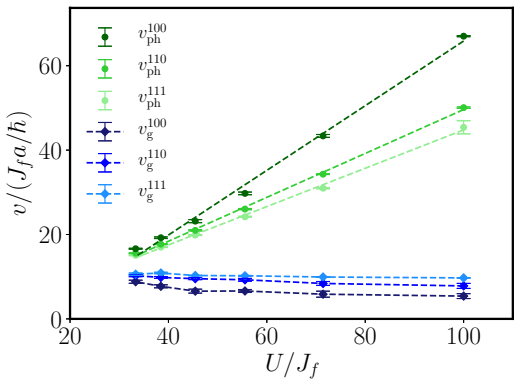

FIG. 6. Phase velocity ($v_{\rm ph}$) and group velocity ($v_{\rm g}$) along the (1,0,0), (1,1,0), and (1,1,1) directions as a function of U/J_f for the BHM in three dimensions.

$28 \times 28 \times 28$ lattice with PBCs, and the results are illustrated in Fig. 6. The group velocity is relatively insensitive to U/J_f, as found in Ref. [41], whereas the phase velocity increases approximately linearly with U/J_f. Similarly to two dimensions, there is also anisotropy in both the group and phase velocities which decreases as the critical point is approached, and it has the opposite sense for phase and group velocities. The group velocity is maximal along the (1,1,1) direction and the phase velocity is minimal along the same direction at a given U/J_f.

IV. DISCUSSION AND CONCLUSIONS

We have applied our 2PI strong-coupling approach to the BHM to calculate the spreading of single-particle correlations and found excellent agreement with experiments in one [12,21] and two [12] dimensions. This establishes our 2PI strong-coupling approach as a powerful tool to study out-of-equilibrium dynamics in the BHM in dimensions greater than one. Given that the method gives more accurate results for equilibrium properties, such as phase boundaries, with increasing dimension [40], we expect the same to be true for out-of-equilibrium dynamics. Hence, as it reproduces exact results in one dimension, the 2PI method is complementary to numerical methods that give essentially exact results for out-of-equilibrium dynamics only in one dimension. In addition, the 2PI method can be extended to disordered systems [42,44] and multicomponent boson systems. We have also demonstrated anisotropy in the spreading of correlations on a lattice in both two and three dimensions. This anisotropy persists throughout the entire Mott phase, apparently vanishing only around the critical point. Our results for the phase velocity and group velocity as a function of U/J_f demonstrate that, while they are relatively similar in the vicinity of the transition to the superfluid, deeper in the Mott phase there can be very significant differences, with the phase velocity being much larger than the group velocity. Differentiating between these two velocities is important for understanding the rate of information spreading in the BHM. At the present time there have been only a few measurements of the velocities at which correlations spread in the BHM, and we hope that our results give an incentive to further experimental measurements of correlation spreading in the BHM.

ACKNOWLEDGMENTS

A.M.-J. and M.K. acknowledge support from NSERC, and M.F. was supported by a Mitacs Accelerate Postdoctoral Fellowship. The authors thank Y. Takasu for helpful correspondence and J. McGuirk and R. Wortis for thoughtful comments on the paper.

APPENDIX A: REAL-TIME TWO-PARTICLE IRREDUCIBLE APPROACH TO THE BOSE-HUBBARD MODEL

In this Appendix we provide a brief summary of our real-time two-particle irreducible (2PI) approach to the Bose-Hubbard model developed in Refs. [40,41]. We then give a brief review of the equations of motion we solve.

We use a contour-time formalism, making use of the Konstantinov-Perel (KP) [45] contour, illustrated in Fig. 7. Fields are labeled according to their contour, which can be $+$, $-$, or $\mathcal{T}$, and we use the notation $\hat{a}^a_{\mathbf{r}_i\alpha}$ for bosonic fields on site i (located at position $\mathbf{r}_i$) and contour α where $\hat{a}^1_{\mathbf{r}_i\alpha} = \hat{a}_{\mathbf{r}_i\alpha}$ and $\hat{a}^2_{\mathbf{r}_i\alpha} = \hat{a}^\dagger_{\mathbf{r}_i\alpha}$. We cast the generating functional $\mathcal{Z}$ for the Bose-Hubbard model in path integral form (omitting source terms),

$$\mathcal{Z} = \int [\mathcal{D}a] e^{iS_{\rm BHM}[a]}, \tag{A1}$$

where $S_{\rm BHM}[a]$ is the action for the Bose-Hubbard model.

We perform two Hubbard-Stratonovich transformations on the BHM action [39–41,46] and then perform a cumulant expansion to quartic order, which gives the following action [40]:

$$S_{\rm BHM}[z] = \frac{1}{2!}\left(2J_{x_1x_2} + [\mathcal{G}^{-1}]_{x_1x_2} + \tilde{u}_{x_1x_2}\right) z_{x_1} z_{x_2} + \frac{1}{4!} u_{x_1\ldots x_4} z_{x_1} z_{x_2} z_{x_3} z_{x_4}, \tag{A2}$$

where the z fields can be shown to have the same correlations as the original a fields [40,46]. We make use of the Einstein summation convention and introduce highly condensed notation so that for a quantity Q,

$$Q_{x_1x_2\ldots x_n} = Q^{a_1a_2\ldots a_n}_{\mathbf{r}_{i_1}\mathbf{r}_{i_2}\ldots\mathbf{r}_{i_n},\alpha_1\alpha_2\ldots\alpha_n}(s_1, s_2, \ldots, s_n), \tag{A3}$$

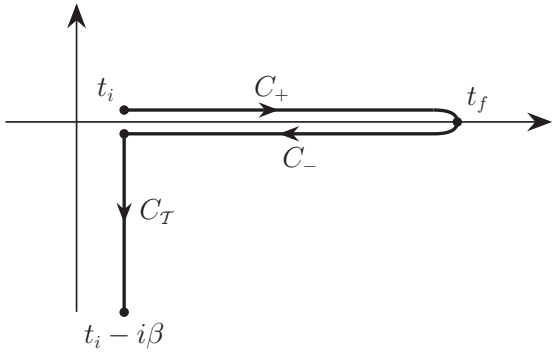

FIG. 7. KP contour used in calculations. The system is taken to be prepared in an initially thermal state at time t_i and then evolved to a final time t_f.

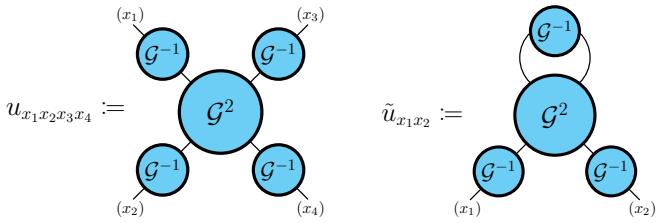

FIG. 8. The four-point vertex u and the two-point vertex $\tilde{u}$ in the effective theory.

where α_i is a contour label, $\mathbf{r}_{i_n}$ is a lattice site position, and s_i is a non-negative real parameter that indicates a position along the contour segment C_{α_i}. The u vertex is nonlocal in time and generates "physical" and "anomalous" diagrams (i.e., those with internal lines of $\mathcal{G}^{-1}$). The $\tilde{u}$ vertex cancels anomalous terms generated by u vertices, and $\mathcal{G}$ and $\mathcal{G}^2$ are connected 1- and 2-particle Green's functions in the atomic limit ($J = 0$). These vertices are illustrated in Fig. 8. Full details of the expressions for each of these vertices are presented in Ref. [40]. With the effective theory defined by Eq. (A2) we can construct the 2PI effective action from whence we obtain equations of motion.

Two-particle irreducible equations of motion

With the effective theory defined by Eq. (A2) we can construct the 2PI effective action and hence obtain the 2PI equations of motion [37]. The equations of motion for the superfluid order parameter ϕ and the propagator G take the form

$$\frac{\delta S[\phi]}{\delta \phi_x} + \frac{1}{2}\left[i \frac{\delta [D^{-1}]_{x_1x_2}}{\delta \phi_x} G_{x_2x_1} \right] + \frac{\delta \Gamma_2[\phi, G]}{\delta \phi_x} = 0, \tag{A4}$$

and

$$i[G^{-1}]_{x_1x_2} = i[D^{-1}]_{x_1x_2} - i\Sigma_{x_1x_2}, \tag{A5}$$

where Eq. (A5) is the Dyson's equation, $i[D^{-1}]$ is the inverse "bare" propagator, and Σ is the 2PI self-energy:

$$i[D^{-1}]_{x_1x_2} \equiv \frac{\delta^2 S[\phi]}{\delta \phi_{x_1} \delta \phi_{x_2}}, \quad \Sigma_{x_1x_2} \equiv 2i \frac{\delta \Gamma_2[\phi, G]}{\delta G_{x_1x_2}}. \tag{A6}$$

The 2PI self-energy is obtained from a functional derivative of Γ_2 which is represented diagrammatically to second order in the interaction vertex in Fig. 9.

The equations of motion obtained from Eqs. (A4) and (A5) when including diagrams a, b, and c in Γ_2 can have as many as seven time integrals. Hence we make several approximations to obtain equations that are more amenable to numerical solution. First, we make the Hartree-Fock Bogoliubov (HFB)

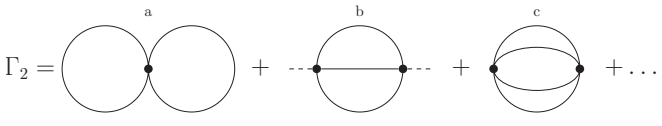

FIG. 9. Diagrammatic expansion of Γ_2. The interaction vertex u is represented by a bullet •, the propagator G is represented by a solid line, and the superfluid order parameter ϕ is represented by a dashed line.

approximation [41] and keep only diagram a in Γ_2. Second, we make a low-frequency approximation. This allows the vertices u and $\tilde{u}$ to be replaced by constants u_1, u_2, and v_1, details of which are given in Refs. [40,41]. Terms involving u_2 can be shown to be small in comparison to those involving u_1, and hence after following through these simplifications, as outlined in Refs. [40,41] we obtain equations of motion for the spectral function

$$A_{\mathbf{k}}(t, t') = \langle \hat{a}_{\mathbf{k}}(t) \hat{a}^\dagger_{\mathbf{k}}(t') - \hat{a}^\dagger_{\mathbf{k}}(t') \hat{a}_{\mathbf{k}}(t) \rangle_{\hat{\rho}_i}, \tag{A7}$$

and the kinetic Green's function

$$G^{(K)}_{\mathbf{k}}(t, t') = -i \langle \hat{a}_{\mathbf{k}}(t) \hat{a}^\dagger_{\mathbf{k}}(t') + \hat{a}^\dagger_{\mathbf{k}}(t') \hat{a}_{\mathbf{k}}(t) \rangle_{\hat{\rho}_i}, \tag{A8}$$

where the expectation values are taken with respect to the initial state

$$\hat{\rho}_i = \frac{e^{-\beta \hat{H}_{\mathrm{BHM}}(t_i)}}{\mathrm{Tr}[e^{-\beta \hat{H}_{\mathrm{BHM}}(t_i)}]}. \tag{A9}$$

For a quench that leads to a final state in the Mott-insulating regime and in which the system is initially thermalized in the atomic limit ($J = 0$), the equations of motion take the form [41]

$$A_{\mathbf{k}}(t, t') = \mathcal{A}(t - t') - i \int_{t'}^{t} dt'' \mathcal{A}(t - t'') \Sigma^{(\mathrm{HFB})}_{\mathbf{k}}(t'') A_{\mathbf{k}}(t'', t'), \tag{A10}$$

$$G^{(K)}_{\mathbf{k}}(t, t') = \mathcal{G}^{(K)}(t - t') - i \int_{0}^{t} dt'' \mathcal{A}(t - t'') \Sigma^{(\mathrm{HFB})}_{\mathbf{k}}(t'') G^{(K)}_{\mathbf{k}}(t'', t') + i \int_{0}^{t'} dt'' \mathcal{G}^{(K)}(t - t'') \Sigma^{(\mathrm{HFB})}_{\mathbf{k}}(t'') A_{\mathbf{k}}(t'', t'), \tag{A11}$$

where $\mathcal{A}(t - t')$ and $\mathcal{G}^{(K)}(t - t')$ are the spectral function and the kinetic Green's function in the atomic ($J = 0$) limit (in this limit both quantities are time translation invariant). Specific forms for $\mathcal{A}$ and $\mathcal{G}^{(K)}$ are specified in Refs. [40,41]. The Hartree-Fock-Bogoliubov-like approximation for the self-energy (obtained by only keeping diagram a of Γ_2) takes the form

$$\Sigma^{(\mathrm{HFB})}_{\mathbf{k}}(t) = \epsilon_{\mathbf{k}}(t) + 2u_1[n(t) - n_{J=0}], \tag{A12}$$

with

$$\epsilon_{\mathbf{k}} = -2J(t) \sum_{i=1}^{d} \cos(k_i a), \tag{A13}$$

$$n(t) = \frac{1}{N_s} \sum_{\mathbf{k}} n_{\mathbf{k}}(t), \tag{A14}$$

$$n_{\mathbf{k}}(t) = \frac{1}{2}\left\{ i G^{(K)}_{\mathbf{k}}(t, t) - 1 \right\}, \tag{A15}$$

and u_1 depends on U, μ, and temperature [40]. Knowledge of $n_{\mathbf{k}}(t)$—the particle distibution over the quasimomentum $\mathbf{k}$ at time t—allows us to calculate the single-particle density

matrix. The full expression for u_1 is

$$u_1 = -\frac{2\{\mathcal{G}^{12,(R)}(\omega'=0)\}^{-4}}{\mathcal{Z}_0}\sum_{n=0}^{\infty} e^{-\beta(\mathcal{E}_n-\mathcal{E}_{n_0})}\left\{\frac{(n+1)(n+2)}{(\mathcal{E}_{n+2}-\mathcal{E}_n)(\mathcal{E}_{n+1}-\mathcal{E}_n)^2}+\frac{n(n-1)}{(\mathcal{E}_{n-2}-\mathcal{E}_n)(\mathcal{E}_{n-1}-\mathcal{E}_n)^2}\right.$$
$$\left.-\frac{(n+1)^2}{(\mathcal{E}_{n+1}-\mathcal{E}_n)^3}-\frac{n^2}{(\mathcal{E}_{n-1}-\mathcal{E}_n)^3}-\frac{n(n+1)}{(\mathcal{E}_{n+1}-\mathcal{E}_n)(\mathcal{E}_{n-1}-\mathcal{E}_n)^2}-\frac{n(n+1)}{(\mathcal{E}_{n+1}-\mathcal{E}_n)^2(\mathcal{E}_{n-1}-\mathcal{E}_n)}\right\}, \tag{A16}$$

where

$$\mathcal{G}^{12,(R)}(\omega'=0) = -\frac{1}{\mathcal{Z}_0}\sum_{n=0}^{\infty} e^{-\beta(\mathcal{E}_n-\mathcal{E}_{n_0})}\left\{\frac{(n+1)}{\mathcal{E}_{n+1}-\mathcal{E}_n}+\frac{n}{\mathcal{E}_{n-1}-\mathcal{E}_n}\right\}, \tag{A17}$$

and $\mathcal{Z}_0$ is the atomic partition function,

$$\mathcal{Z}_0 \equiv \sum_{n=0}^{\infty} e^{-\beta(\mathcal{E}_n-\mathcal{E}_{n_0})}, \tag{A18}$$

with $n_0 = \lceil \mu/U \rceil$ and

$$\mathcal{E}_n = \frac{U}{2}n(n-1) - n\mu. \tag{A19}$$

The Hartree-Fock-Bogoliubov self-energy is most accurate in the strongly interacting limit and is least accurate at the tips of the Mott lobes. This is illustrated in Fig. 6 of Ref. [40], where phase boundaries between the Mott and superfluid phases were calculated with the HFB self-energy and compared with both mean-field theory and exact numerical results. In dimensions 1, 2, and 3, the HFB self-energy leads to a significant improvement beyond mean-field theory, and in dimensions 2 and 3 it is only at the tips of the Mott lobes where there is some deviation between exact and HFB results. The deviations in 1 dimension are larger, but even there the HFB result is a dramatic improvement on mean-field theory.

The explicit form of $J(t)$ that we consider is

$$J(t) = \frac{J_f}{2}\left[1+\tanh\left(\frac{t-t_c}{\tau_Q}\right)\right], \tag{A20}$$

where J_f characterizes the final hopping strength, t_c characterizes the time at which the middle of the quench occurs, and τ_Q characterizes the duration of the quench. The equations of motion do not have any known analytical solution, and hence we have solved them numerically using a block-by-block

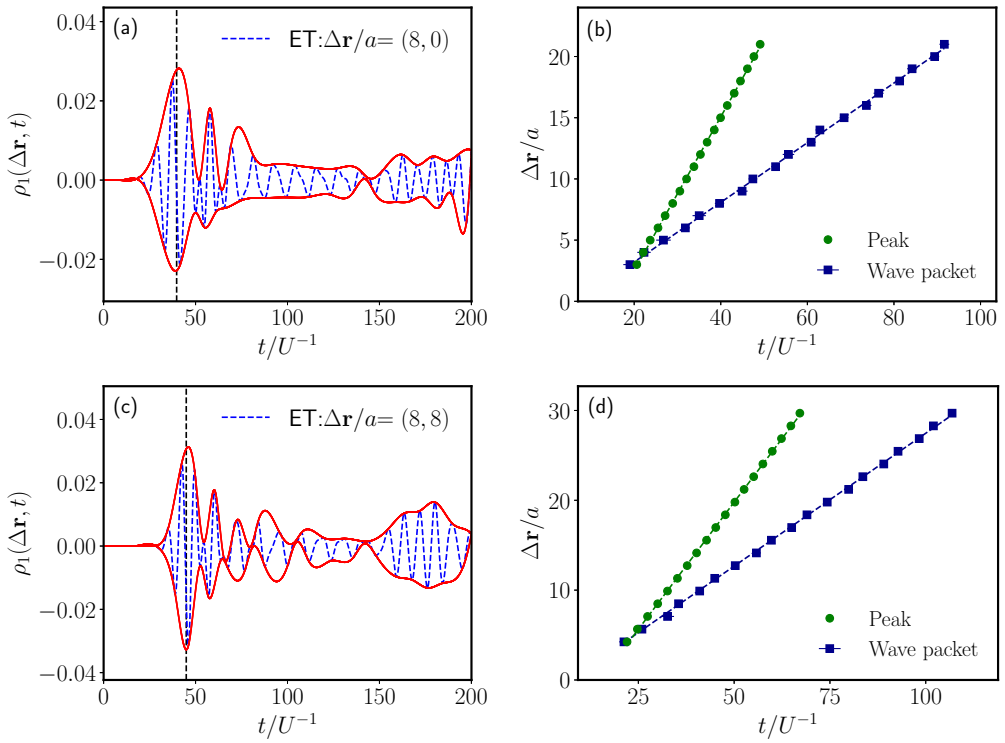

FIG. 10. Tracking the wavefront for a 50 × 50 system. (a), (c) Dynamics of $\rho_1(\Delta\mathbf{r}, t)$ for $\Delta\mathbf{r}/a = (8, 0)$ and $\Delta\mathbf{r}/a = (8, 8)$. (b), (d) Scatter plots of the times t/U^{-1} for the maximum peak (green) and the wave packet (blue) to travel a particle separation distance $\Delta r/a$ along the crystal axes and diagonals, respectively. In panels (a) and (c) the solid red lines trace the envelopes of the wave packets, while the dashed black vertical lines indicate the positions of the wave packets. In panels (b) and (d) we fit straight lines to the data to obtain the group and phase velocities along the crystal axes and diagonals. The parameters are $\beta U = 1000$, $U/J_f = 28.6$, $\mu/U = 0.4116$, $t_c/U^{-1} = 5$, $t_Q/U^{-1} = 0.1$.

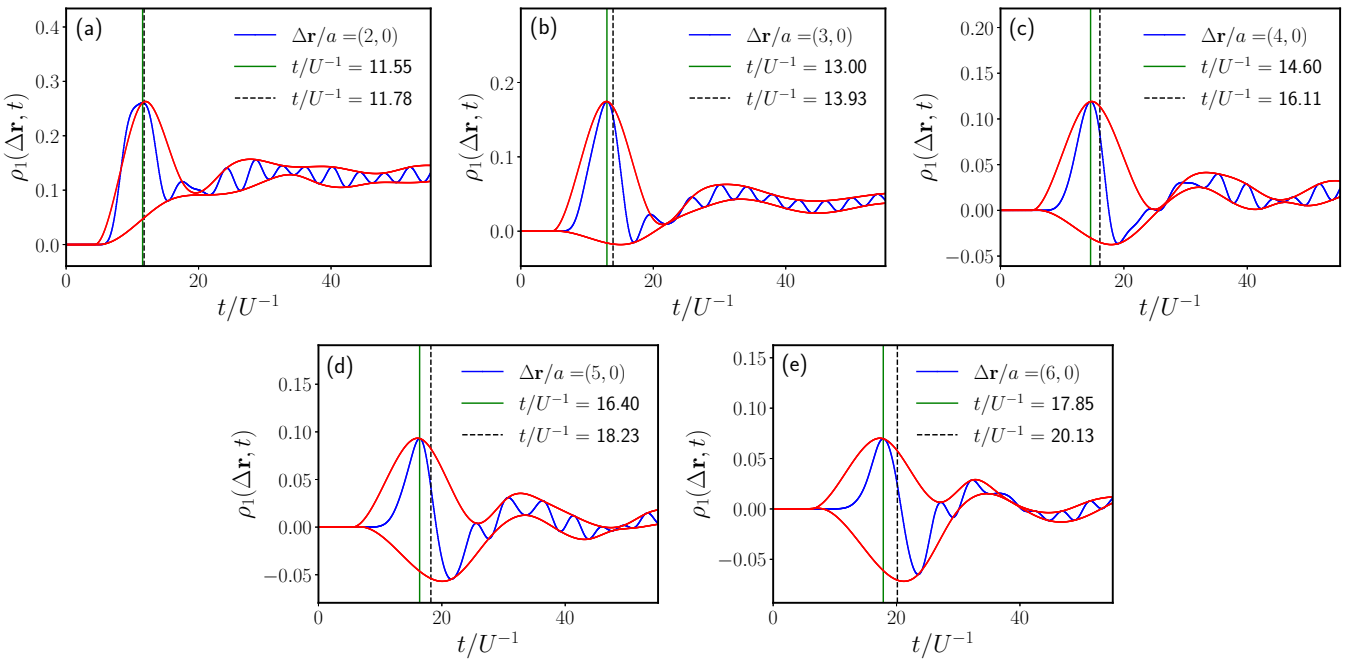

FIG. 11. (a)–(e) Dynamics of $\rho_1(\Delta\mathbf{r}, t)$ along the crystal axis from $\Delta\mathbf{r}/a = (2, 0)$ to $\Delta\mathbf{r}/a = (6, 0)$. The solid vertical green lines show the positions of the peaks related to the phase velocity and dashed vertical black lines show the positions of the wave packets related to group velocity. The parameters in panels (a) and (e) are $\beta U = 1000$, $U/J_f = 19.6$, $\mu/U = 0.4116$, $t_c/U^{-1} = 5$, $t_Q/U^{-1} = 0.1$, and the system size is 50×50.

scheme detailed in Ref. [41]. We give additional details about the solutions of these equations in the following section.

APPENDIX B: SINGLE-PARTICLE CORRELATIONS

In this Appendix we provide additional details relating to the methodology we used to identify the group velocity and phase velocity for the spreading of correlations from our calculations of $\rho_1(\Delta\mathbf{r}, t)$. We discussed the one-dimensional case in the main body of the paper but provide additional details for the two- and three-dimensional cases here. For a given U/J_f, we calculate $\rho_1(\Delta\mathbf{r}, t)$ and for each value of $\Delta\mathbf{r}$ we obtain the time-wise positions of the wave packet, and the largest peak [i.e., the point in time where $\rho_1(\Delta\mathbf{r}, t)$ takes its maximum value].

We track the propagation of the maximum peak of the $\rho_1(\Delta\mathbf{r}, t)$ time series to extract the phase velocity. For the group velocity we first locate all local maxima and minima of $\rho_1(\Delta\mathbf{r}, t)$ and then use these points to construct upper

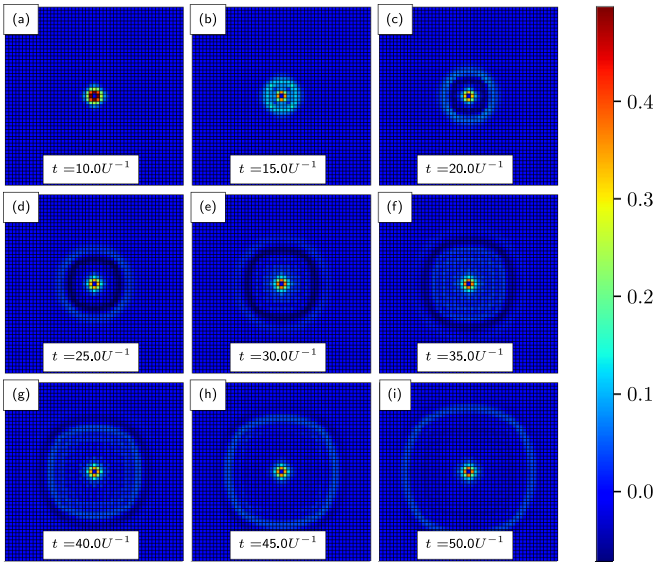

FIG. 12. (a)–(i) Spatial dependency of $\rho_1(\Delta\mathbf{r}, t)$ at different moments in time t/U^{-1} for a 50×50 site system. The parameters used are $\beta U = 1000$, $U/J_f = 19.6$, $\mu/U = 0.4116$, $t_c/U^{-1} = 5$, $t_Q/U^{-1} = 0.1$.

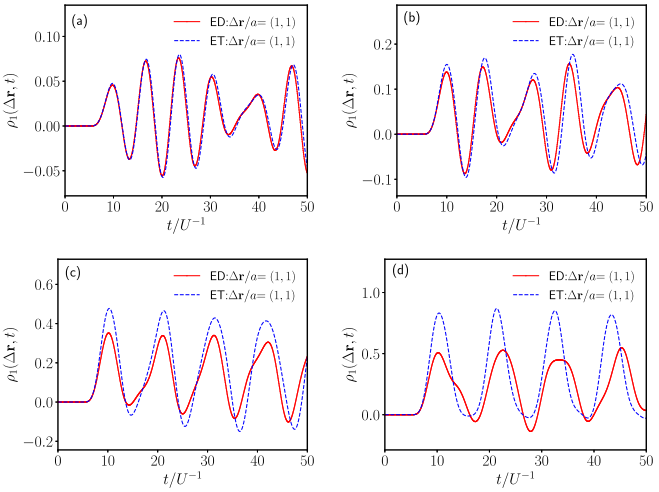

FIG. 13. Comparison of exact diagonalization (ED) calculations and effective theory (ET) calculations of $\rho_1(\Delta\mathbf{r}, t)$ for $\Delta\mathbf{r}/a = (1, 1)$ for interaction strengths (a) $U/J_f = 66.7$, (b) $U/J_f = 40$, (c) $U/J_f = 25$, and (d) $U/J_f = 19.6$. The parameters are $\beta U = 1000$, $\mu/U = 0.4116$, $t_c/U^{-1} = 5$, $t_Q/U^{-1} = 0.1$.

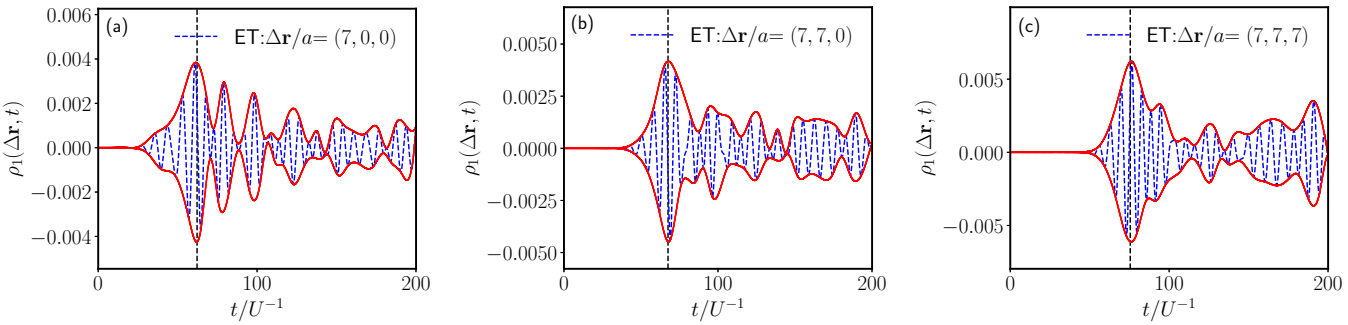

FIG. 14. Tracking the wavefront in a $28 \times 28 \times 28$ system. Dynamics of $\rho_1(\Delta\mathbf{r}, t)$ for (a) $\Delta\mathbf{r}/a = (7, 0, 0)$, (b) $\Delta\mathbf{r}/a = (7, 7, 0)$, and (c) $\Delta\mathbf{r}/a = (7, 7, 7)$. The solid red lines trace the envelopes of the wave packets, while the dashed black vertical lines indicate the positions of the wave packets. The parameters are $\beta U = 1000$, $U/J_f = 55.6$, $\mu/U = 0.4116$, $t_c/U^{-1} = 5$, $t_Q/U^{-1} = 0.1$.

and lower envelopes using both linear and cubic interpolation. Having found two different pairs of upper and lower envelopes, one from the linear interpolation and one from the cubic interpolation, we find the times $t_{\max}$ and $t_{\min}$ where each envelope has a maximum or minimum, respectively. To find the center of the wave packet we average $t_{\max}$ and $t_{\min}$ in three different ways, for each pair of upper and lower envelopes (i.e., we consider six different estimates for the center of the wave packet).

The averages we consider are

$$C_1 = \frac{t_{\max} + t_{\min}}{2}, \tag{B1}$$

and

$$C_2 = \frac{\alpha t_{\max} + \beta t_{\min}}{\alpha + \beta}, \tag{B2}$$

where $\alpha = |\rho_{\max} - \rho_{\text{av}}|$ and $\beta = |\rho_{\text{av}} - \rho_{\min}|$, with $\rho_{\max}$ the maximum value of $\rho_1(\Delta\mathbf{r}, t)$, $\rho_{\min}$ the minimum value of $\rho_1(\Delta\mathbf{r}, t)$ and ρ_{av} the average of $\rho_1(\Delta\mathbf{r}, t)$. We calculate C_2 with (i) ρ_{av} averaged over the whole time interval and (ii) with ρ_{av} averaged over the time interval $[0, t_{\max} + 5U^{-1}]$ (to capture the average of $\rho_1(\Delta\mathbf{r}, t)$ in the only the first peak). We then average C_1 and the two different versions of C_2 for both sets of envelopes to determine the center of the envelope. These multiple approaches allow us to estimate the uncertainty in the center of the envelope, which is generally small, e.g., see Figs. 10(b) and 10(d). By tracking the propagation of the wave packet, we can extract the group velocity for the spreading of single-particle correlations [41].

In Figs. 10(a) and 10(c) we display the time evolution of $\rho_1(\Delta\mathbf{r}, t)$ for $\Delta\mathbf{r}/a = (8, 0)$ (i.e., along the crystal axis) and $\Delta\mathbf{r}/a = (8, 8)$ (i.e., along the diagonal), respectively. Figures 10(b) and 10(d) plot the times t/U^{-1} for the maximum peak and the wave packet to travel a particle separation distance $\Delta r/a$ along the crystal axes [Fig. 10(b)] and diagonals [Fig. 10(d)], respectively. The calculations are for $U/J_f = 28.6$ and a 50×50 lattice.

Similarly to the one-dimensional case, we calculate $\rho_1(\Delta\mathbf{r}, t)$ for a variety of U/J_f in the Mott phase and calculate the phase and group velocities for correlation spreading. To illustrate the process of determining the phase and group velocities more clearly, in Fig. 11 we show snapshots of $\rho_1(\Delta\mathbf{r}, t)$ from $\mathbf{r}/a = (2, 0)$ to $\mathbf{r}/a = (6, 0)$ along the crystal axis. For each plot, we mark the time-wise positions of the maximum peak and the wave packet by vertical solid green and vertical dashed black lines, respectively. The increasing gap between the two lines with increasing distance along the crystal axis illustrates the difference between the group and phase velocities.

In Ref. [12] the authors used both peaks and troughs to determine the phase velocity of excitations. In Fig. 12 we illustrate the spreading of correlations in two dimensions for $U/J_f = 19.6$. Peaks are visible as light blue circles and troughs are visible as dark blue circles. There is some anisotropy in the spreading, but it is relatively small since the value of U/J_f is close to the critical value.

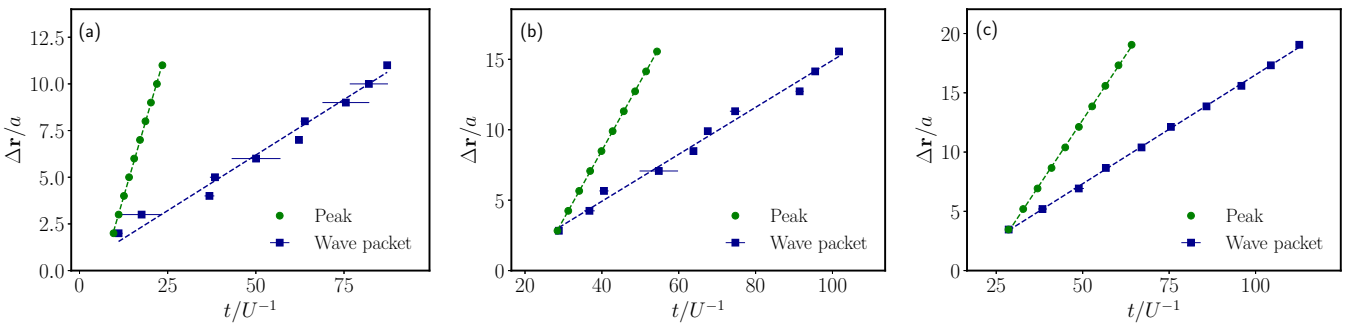

FIG. 15. Scatter plots of the time t/U^{-1} for the maximum peak (green) and the wave packet (blue) to travel a distance $\Delta r/a$ along (a) the (1,0,0) direction, (b) the (1,1,0) direction, and (c) the (1,1,1) direction. Parameters are the same as in Fig. 14.

As a test of our approach in two dimensions, we performed exact diagonalization calculations on a 3×3 system and compared the results for $\rho_1(\Delta\mathbf{r}, t)$ with the results of our effective theory. The comparisons between both methods are shown in Fig. 13. We find that the quantitative agreement between the effective theory and ED is excellent at large values of U/J_f, but becomes less accurate for values of U/J_f close to the transition, where there is a discrepancy in the magnitude of $\rho_1(\Delta\mathbf{r}, t)$ by roughly a factor of two. However, the phase of $\rho_1(\Delta\mathbf{r}, t)$, in particular, the position of the first peak, is represented accurately by the effective theory.

We also give a sample of some of the calculations of $\rho_1(\Delta\mathbf{r}, t)$ we calculated for three dimensions, showing traces of $\rho_1(\Delta\mathbf{r}, t)$ along three different crystal directions in Fig. 14 and fits used to determine the group and phase velocities along the respective directions for $U/J_f = 55.6$ in Fig. 15.

[1] M. Greiner, O. Mandel, T. Esslinger, T. W. Hänsch, and I. Bloch, Nature (London) **415**, 39 (2002).
[2] I. Bloch, Nat. Phys. **1**, 23 (2005).
[3] M. Lewenstein, A. Sanpera, V. Ahufinger, B. Damski, A. Sen, and U. Sen, Adv. Phys. **56**, 243 (2007).
[4] I. Bloch, J. Dalibard, and W. Zwerger, Rev. Mod. Phys. **80**, 885 (2008).
[5] C.-L. Hung, X. Zhang, N. Gemelke, and C. Chin, Phys. Rev. Lett. **104**, 160403 (2010).
[6] D. Chen, M. White, C. Borries, and B. DeMarco, Phys. Rev. Lett. **106**, 235304 (2011).
[7] M. P. Kennett, ISRN Condens. Matter Phys. **2013**, 393616 (2013).
[8] C. Gross and I. Bloch, Science **357**, 995 (2017).
[9] M. P. A. Fisher, P. B. Weichman, G. Grinstein, and D. S. Fisher, Phys. Rev. B **40**, 546 (1989).
[10] D. Jaksch, C. Bruder, J. I. Cirac, C. W. Gardiner, and P. Zoller, Phys. Rev. Lett. **81**, 3108 (1998).
[11] J.-Y. Choi, S. Hild, J. Zeiher, P. Schauß, A. Rubio-Abadal, T. Yefsah, V. Khemani, D. A. Huse, I. Bloch, and C. Gross, Science **352**, 1547 (2016).
[12] Y. Takasu, T. Yagami, H. Asaka, Y. Fukushima, K. Nagao, S. Goto, I. Danshita, and Y. Takahashi, Sci. Adv. **6**, eaba9255 (2020).
[13] S. Bose, Contemp. Phys. **48**, 13 (2007).
[14] E. H. Lieb and D. W. Robinson, Commun. Math. Phys. **28**, 251 (1972).
[15] B. Nachtergaele, H. Raz, B. Schlein, and R. Sims, Commun. Math. Phys. **286**, 1073 (2009).
[16] J. Eisert and D. Gross, Phys. Rev. Lett. **102**, 240501 (2009).
[17] J. Jünemann, A. Cadarso, D. Pérez-García, A. Bermudez, and J. J. García-Ripoll, Phys. Rev. Lett. **111**, 230404 (2013).
[18] N. Schuch, S. K. Harrison, T. J. Osborne, and J. Eisert, Phys. Rev. A **84**, 032309 (2011).
[19] W. S. Bakr, A. Peng, M. E. Tai, R. Ma, J. Simon, J. I. Gillen, S. Fölling, L. Pollet, and M. Greiner, Science **329**, 547 (2010).
[20] J. F. Sherson, C. Weitenberg, M. Endres, M. Cheneau, I. Bloch, and S. Kuhr, Nature (London) **467**, 68 (2010).
[21] M. Cheneau, P. Barmettler, D. Poletti, M. Endres, P. Schauß, T. Fukuhara, C. Gross, I. Bloch, C. Kollath, and S. Kuhr, Nature (London) **481**, 484 (2012).
[22] S. R. Clark and D. Jaksch, Phys. Rev. A **70**, 043612 (2004).
[23] C. Kollath, A. M. Läuchli, and E. Altman, Phys. Rev. Lett. **98**, 180601 (2007).
[24] A. M. Läuchli and C. Kollath, J. Stat. Mech. (2008) P05018.
[25] J.-S. Bernier, G. Roux, and C. Kollath, Phys. Rev. Lett. **106**, 200601 (2011).
[26] J.-S. Bernier, D. Poletti, P. Barmettler, G. Roux, and C. Kollath, Phys. Rev. A **85**, 033641 (2012).
[27] P. Barmettler, D. Poletti, M. Cheneau, and C. Kollath, Phys. Rev. A **85**, 053625 (2012).
[28] S. Trotzky, Y.-A. Chen, A. Flesch, I. P. McCulloch, U. Schollwöck, J. Eisert, and I. Bloch, Nat. Phys. **8**, 325 (2012).
[29] L. Cevolani, J. Despres, G. Carleo, L. Tagliacozzo, and L. Sanchez-Palencia, Phys. Rev. B **98**, 024302 (2018).
[30] J. Despres, L. Villa, and L. Sanchez-Palencia, Sci. Rep. **9**, 4135 (2019).
[31] P. Navez and R. Schützhold, Phys. Rev. A **82**, 063603 (2010).
[32] C. Trefzger and K. Sengupta, Phys. Rev. Lett. **106**, 095702 (2011).
[33] K. V. Krutitsky, P. Navez, F. Quiesser, and R. Schützhold, Eur. Phys. J. Quantum Tech. **1**, 12 (2014).
[34] F. Queisser, K. V. Krutitsky, P. Navez, and R. Schützhold, Phys. Rev. A **89**, 033616 (2014).
[35] G. Carleo, F. Becca, L. Sanchez-Palencia, S. Sorella, and M. Fabrizio, Phys. Rev. A **89**, 031602(R) (2014).
[36] Y. Yanay and E. J. Mueller, Phys. Rev. A **93**, 013622 (2016).
[37] J. M. Cornwall, R. Jackiw, and E. Tomboulis, Phys. Rev. D **10**, 2428 (1974).
[38] J. Berges, in *IX Hadron Physics and VII Relativistic Aspects of Nuclear Physics: A Joint Meeting on QCD and QCP*, edited by M. Bracco, M. Chiapparini, E. Ferreira, and T. Kodama, AIP Conf. Proc. 739 (AIP, New York, 2004).
[39] M. P. Kennett and D. Dalidovich, Phys. Rev. A **84**, 033620 (2011).
[40] M. R. C. Fitzpatrick and M. P. Kennett, Nucl. Phys. B **930**, 1 (2018).
[41] M. R. C. Fitzpatrick and M. P. Kennett, Phys. Rev. A **98**, 053618 (2018).
[42] M. P. Kennett and M. R. C. Fitzpatrick, J. Low Temp. Phys. **201**, 82 (2020).
[43] G. Stefanucci and R. van Leeuwen, *Nonequilibrium Many-Body Theory of Quantum Systems* (Cambridge University Press, New York, 2013).
[44] M. R. C. Fitzpatrick, Ph.D. thesis, Simon Fraser University, 2019.
[45] O. V. Konstantinov and V. I. Perel, Zh. Eksp. Teor. Fiz. **39**, 197 (1961) [Sov. Phys. JETP **12**, 142 (1961)].
[46] K. Sengupta and N. Dupuis, Phys. Rev. A **71**, 033629 (2005).